Langmuir

Article

pubs.acs.org/Langmuir

Synaptosomal Membrane-Based Langmuir–Blodgett Films: A Platform for Studies on γ-Aminobutyric Acid Type A Receptor Binding Properties

Anahí V. Turina, Pedro D. Clop, and María A. Perillo*

Instituto de Investigaciones Biológicas y Tecnológicas, IIByT, (CONICET- UNC), Cátedra de Química Biológica, Facultad de Ciencias Exactas, Físicas y Naturales, Universidad Nacional de Córdoba, Av. Vélez Sarsfield 1611, 5016 Córdoba, Argentina

Supporting Information

ABSTRACT: In this work we used Langmuir–Blodgett films (LB) as model membranes to study the effect of molecular packing on the flunitrazepam (FNZ) accessibility to the binding sites at the $GABA_A$ receptor ($GABA_A$-R). Ligand binding data were correlated with film topography analysis by atomic force microscopy images (AFM) and SDS-PAGE. Langmuir films (LF) were prepared by the spreading of synaptosomal membranes (SM) from bovine brain cortex at the air–water interface. LBs were obtained by the transference, at 15 or 35 mN/m constant surface pressure (π), of one ($LB_{15/1c}$ and $LB_{35/1c}$) or two ($LB_{35/2c}$) LFs to a film-free hydrophobic alkylated substrate (CON_{glass}). Transference was performed in a serial manner, which allowed the accumulation of a great number of samples. SDS-PAGE clearly showed a 55 kDa band characteristic of $GABA_A$-R subunits. Detrended fluctuation analysis of topographic data from AFM images exhibited a single slope value (self-similarity parameter α) in CON_{glass} and a discontinuous slope change in the α value at an autocorrelation length of ~100 nm in all LB samples, supporting the LF transference to the substrate. AFM images of CON_{glass} and $LB_{15/1c}$ exhibited roughness and average heights that were similar between measurements and significantly lower than those of $LB_{35/1c}$ and $LB_{35/2c}$, suggesting that the substrate coverage in the latter was more stable than in $LB_{15/1c}$. While [^{3}H]FNZ binding in $LB_{15/1c}$ did not reach saturation, in $LB_{35/1c}$ the binding kinetics became sigmoid with a binding affinity lower than in the SM suspension. Our results highlight the π dependence of both binding and topological data and call to mind the receptor mechanosensitivity. Thus, LB films provide a tool for bionanosensing $GABA_A$-R ligand binding as well as $GABA_A$-R activity modulation induced by the environmental supramolecular organization.

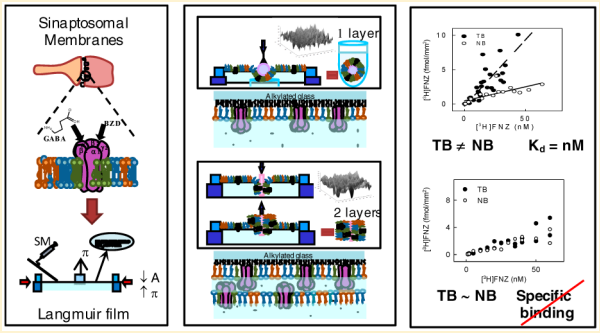

1. INTRODUCTION

It is well documented that a Langmuir film[1] built from amphypatic molecules self-orientated at the air–water interface can be transferred to a solid support without changes[2,3] to form a Langmuir–Blodgett film (LB).[1,4] The latter was the first technique on the molecular scale used for biosensor development or biochemical probe design.[5,6]

The advantages of interfacial Langmuir monolayers and supported LB films in investigating molecular interactions between biomolecules and lipid membrane components or in elaborating on biomimetic membranes as sensing layers, respectively, are widely recognized.[7]

Most works on biochip developments are based on the immobilization of soluble proteins.[7,8] However, up to 30% of the open reading frames in known genomes encode membrane proteins, most of which are molecular targets for around 50–60% of current validated medicines so they remain the principal target for new drug discovery.[9]

Characterizing their interaction with ligands requires the membrane protein to be in its original membrane, reconstituted in a suitable membrane mimetic, or solubilized in a suitable detergent that retains the native structure, conformation, and activity of the protein as much as possible. Furthermore, for biosensor development, this challenge has to be combined with immobilization or capture of the membrane protein on the sensor surface. This has been achieved through covalent attachment by selective chemistry and capture by antibodies or affinity tags combined with solubilization and reconstitution strategies.[10] However, most times it is not the true protein but a molecularly engineered surrogate overexpressed in a heterologous system that is the closest to a natural model that has been reached.

The $GABA_A$ receptor ($GABA_A$-R) is a channel-gated membrane receptor that could be incorporated into a biosensor in the form of a homooligomeric β3 $GABA_A$-R with a Hys_8-tag introduced between amino acids 4 and 5 of the mature β3 protein. This recombinant protein was overexpressed in insect cells, solubilized with a detergent mixture, and attached to the sensor surface through binding to the immobilized antipoly-histidine antibody covalently immobilized on the sensor by

Received: November 4, 2014
Revised: January 9, 2015

DOI: 10.1021/la5042986
Langmuir XXXX, XXX, XXX–XXX

standard amine coupling chemistry. However, this receptor model is far from the native $GABA_A$-R heteropentamer, the activity of which is known to be strongly dependent on the subunit composition,[10] located in an environment type far from that of a membrane bilayer.

Another aspect to be considered is the fact that when activity studies with integral membrane proteins such as receptors are carried out, there are nonspecific interactions (ligand–membrane) that occur at the same time as the specific ligand–receptor interaction. The membrane partitioning of small hydrophobic molecules can change the structural and thermodynamic properties of the bilayer, affecting the protein conformation and then modulating its activity. The hydrophobic thickness in the bilayer, the curvature, the dipole potential, the microviscosity, and the phase coexistence are related to the composition of the membrane, and it has been demonstrated that they can be affected by drug partitioning.[11−14] Besides, changes in the dipole membrane adjustment can modify the activity, insertion, and folding of integral membrane proteins[15,16] as well as the activity of enzymes that use membrane components as substrates[17] or transcription factors that interact with membranes.[18] These phenomena reflect the mechanosensitivity of membrane receptors such as the NMDA receptor[19] and other integral membrane proteins.[20,21]

Benzodiazepines (BZD) are drugs, pharmacologically grouped within the minor tranquilizers and widely used as anxiolytics, hypnotics, and anticonvulsants. They stimulate inhibitory neurotransmission throughout the brain by enhancing the activity of neurotransmitter γ-amino butyric acid (GABA). They are not active per se but potentiate the GABA-mediated chloride currents, binding at a different site that is allosterically related to the GABA binding site,[22] in the $GABA_A$-R.

Due to their lipophilic characteristics, BZDs interact not only with the receptor site but also, through hydrophobic interactions, with the membrane as a whole by a partitioning process located mainly in the polar headgroup region of the biomembranes.[23−26] Taking these results into account, it is expected that the activity of $GABA_A$-R could be modulated by changes induced by the membrane partitioning of small drugs within the receptor surroundings. The studies mentioned above had been performed using a model membrane type (bilayers) that is unable to allow separate topological effects from those induced by the molecular density. The goal of the present work is to discriminate effects exerted by the molecular packing on the BZD accessibility to its binding site at $GABA_A$-R using the LB film model. The [^{3}H]-FNZ binding was determined under conditions of flat constant membrane curvature. Thus, we used LB films prepared for the first time from $GABA_A$-R containing synaptosomal membrane monolayers, formed by one or two monolayers transferred from the air–water interface at constant lateral surface pressure (35 or 15 mN/m). LB samples were subjected to [^{3}H]-FNZ binding assays to test the effects of molecular packing and the number of layers forming the flat films on the receptor binding activity. These films provide a direct means to develop a $GABA_A$-R-based biosensor retaining its whole spectrum of binding capabilities thanks to the actual subunit composition of the receptor protein used and close to the membrane structure of the environment entrapping the protein.

2. EXPERIMENTAL SECTION

2.1. Materials. The BZD diazepam (DZ) was kindly supplied by Products La Roche (Córdoba, Argentina). FNZ labeled with tritium (^{3}H) at the N1 position ([^{3}H]FNZ) was purchased from New England Nuclear Chemistry (E.I. DuPont de Nemours & Co. Inc., Boston, MA, USA). Other drugs and solvents were of analytical grade.

2.2. Synaptosomal Membrane Preparation. Synaptosomal membranes (SMs, Scheme 1A,B) were obtained from the bovine brain cerebral cortex. Meninges were eliminated, the cortex was dissected, and SMs were purified essentially according to the method of Enna and Snyder, modified by Perillo and Arce,[27] and lyophilized

Scheme 1. Preparation of Langmuir Films from Synaptosomal Membranes[a]

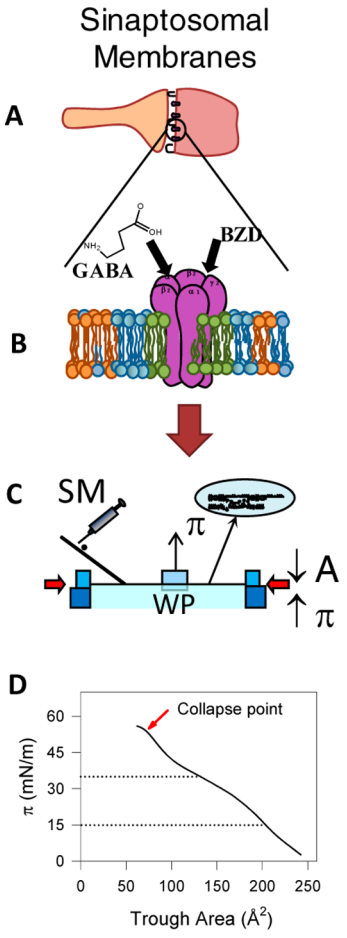

[a](A) Synaptosome (present in the synaptosomal fraction, SF) isolated from bovine brain cortex homogenate as the fraction that precipitates after two-step centrifugation (1000*g* for 10 min and 10 000*g* for 30 min) From the SF, SM are purified as described elseware.[27] (B) $GABA_A$-R is a pentameric membrane-bound protein located in the postsynaptic membrane of the synaptosome. (C) Synaptosomal membrane vesicles (isolated from the postsynaptic membranes of the synaptosomal fraction) are deposited over the air–water interface with the help of a glass rod and spread along the surface, forming the Langmuir film (LF). In moving the barriers, as indicated by the red arrows, the film area (A) decreases, inducing an increase in surface lateral pressure (π) which is measured by the Wilhelmy plate (WP) method. (D) Surface pressure (π)–film area compression isotherm of SM. The collapse point at $\pi = 49 \pm 0.2$ mN/m and $A_{min} = 73 \pm 1$ cm^2 is indicated by the red arrow: dotted lines were drawn at 15 and 35 mN/m and interpolate the isotherm at the points indicated by the arrows. See an enlarged version of the π–A compression isotherm in Figure S1 of the Supporting Information.

DOI: 10.1021/la5042986
Langmuir XXXX, XXX, XXX–XXX

and stored at −20 °C. Immediately before use, membranes were resuspended in 50 mM Tris-HCl buffer (pH 7.4) containing 100 mM NaCl at a final membrane concentration of between 0.25 and 4 mg prot/mL depending on the experiment.

2.3. Langmuir Films. Monomolecular layers were prepared and monitored essentially as described previously.[1,28] Experiments were performed at 22 ± 1 °C. Bidistilled water (230 mL total volume; conductivity 0.01 μS) was used as the subphase. The surface tension of water at 22 °C is 72.45 mN/m.[29] This value is a reference value we check, at the beginning of the experiment, before setting the 0 mN/m and spreading the monolayer. Note that buffer, salts, and other protective agents were absent from the subphase because the effect of this wide variety of chemical species on monolayer properties had not been studied yet. Hence, the subphase composition was kept as simple as possible. For these experiments we used a rectangular trough with a 24 075 mm^2 area, fitted with two Delrin barriers that were moved synchronously by electronic switching. Before each experiment the trough was rinsed and wiped with 70% ethanol and several times with bidistilled water. The absence of surface-active compounds in the pure solvents and in the subphase solution was checked before each run by reducing the available surface area to less than 10% of its original value after enough time was allowed for the adsorption of possible impurities that might have been present in trace amounts. SM monolayers were formed by spreading an aqueous suspension of SM (4 mg prot/mL) over the air−water interface using a glass rod[30] (Scheme 1C). After 10 min, to allow monolayer stabilization, the interface was compressed at a constant rate of 20 mm^2/s. A lower compression rate (12 mm^2/s) was tested, and identical results were obtained. Temperature was maintained with the aid of a water circulating bath.

The surface pressure (π) (Wilhelmy method via a platinized Pt plate) and the area enclosing the monolayer (A) were automatically and continuously recorded with a Minitrough II (KSV, Finland).

Scheme 1D shows a typical π−A compression isotherm obtained from the spreading of 140 μL of the aqueous SM suspension at the air−water interface. The Langmuir film exhibited a collapse pressure of π_c = 49 ± 0.2 mN/m at a minimal area of A_{min} = 73 ± 1 cm^2 and a typical phase transition, usually associated with protein reorganization at the surface.[31]

2.4. Monolayer Transference to Solid Substrates (Langmuir−Blodgett Films). The solid substrate was a 5-mm-diameter glass sphere or circular flat glass (12 mm diameter, 0.15 mm thickness), alkylated with trichloro(octadecyl)silane (OTS). Alkylation conferred to the glass a hydrophobic surface allowing membrane transference at constant lateral pressure (π_{cte}) from an SM monolayer at the air−water interface. Two alkylating methods differing in the solvent used to solubilize OTS (toluene[32] or hexadecane[33]) allowed us to obtain different surface densities of octadecyl groups covalently attached to the glass (greater in the presence of toluene[32]).

Monolayers were transferred to the alkylated glasses at a constant π (35 or 15 mN/m) as described previously.[8] This computer-controlled process started with the alkylated substrate located in the air, above the Langmuir film. When the alkylated glass first dipped through the film, the lipids adhered to the hydrophobic surface through their tails (LB_{1c} sample; Scheme 2A,B). In other cases, after the transference of the first layer, the substrate was extracted from the subphase and a second layer was deposited (LB_{2c} sample), resulting in a double layer with the polar heads of the two facing leaflets having an inner location (Scheme 2C,D). An excellent coverage level of the alkylated substrate was achieved as reflected by the transfer parameters (transfer and cumulative transfer ratio) recorded in real time during monolayer transference to form the LB film (Figure S2 in the Supporting Information). The LB_{2c} samples were stored at 4 °C for not more than 12 h in a humid environment until used. The LB_{1c} samples were built up on glass spheres collected in the subphase (Scheme 2A), manipulated under water to avoid air contact, and conserved at 4 °C for up to 12 h until their use. Previous to the radioligand binding assays (see below), the LB samples were gently washed twice with clean water.

2.5. Atomic Force Microscopy (AFM). The topographic structure of the LB films was evaluated by atomic force microscopy (AFM).[34] The measurements were made on a Multimode NanoScope IIIa AFM, with the sample LB films were submerged in bidistilled water with the following settings: tapping mode, 2 Hz scan frequency, 100 μm pyramidal quartz cantilever, 0.32 N/m nominal value of the spring constant, 0.33 integral gain (IG), and 0.78 proportional gain (PG). Images were flattened (planar fitting) using the software provided by the manufacturer. The topographic structure of the microscopic whole images was first evaluated with the aid of SPIP v.6.3.3, Image Metrology A/S, Hørsholm, Denmark. The parameter superficial roughness (R_a) was estimated using eq 1.

$$R_a = \frac{1}{MN}\sum_{k=0}^{M-1}\sum_{l=0}^{N-1}|z(x_k, y_l) - \mu| \quad (1)$$

The fractal dimension (D_F) was calculated for the different angles from the Fourier angular spectra on a log(amplitude) versus log(frequency) graph. The Fourier angular spectrum depicted in a polar plot is applied to show the fractal dimension as a function of direction. D_F for each direction was calculated from D_F = 3 − (slope/2) (calculated with SPIP v 6.3.3). If the surface is fractal, then the log−log graph will be a straight line with a negative slope. H_m is the maximum height in the

Scheme 2. Langmuir−Blodgett Film Preparation[a]

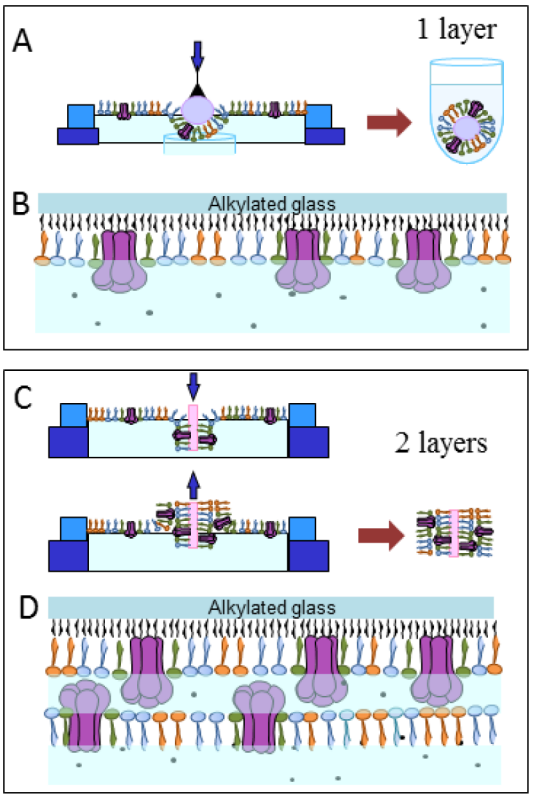

[a](A) An alkylated glass ball gently crosses the Langmuir film, is covered with a one-film layer (Langmuir−Blodgett film), and is received inside a tube submerged in the aqueous subphase, avoiding exposure to air. At the top, a 3D topographic image of the LB film obtained by AFM is shown. (B) Schematic illustration of the $GABA_A$-R-containing LB film immobilized through noncovalent interactions with the alkyl tails covalently attached to the glass surface. The $GABA_A$-R is facing the aqueous media. (C) An alkylated glass coverslip gently crosses the Langmuir film from top to bottom and then from bottom to top and becomes covered with a two-film layer (Langmuir−Blodgett film). (D) Schematic illustration of the $GABA_A$-R-containing two-layer LB film, with one layer immobilized through noncovalent interactions with the alkyl tails covalently attached to the glass surface and the second layer stabilized through noncovalent interaction with the other LB layer. $GABA_A$-R is facing the aqueous interlayer media.

DOI: 10.1021/la5042986
Langmuir XXXX, XXX, XXX−XXX

image. However, it has been reported that R_a and mainly the root-mean-square-based roughness calculation (R_{RMS}) is in general scale-dependent, i.e., it increases with the scanning area, and such a dependence makes it difficult to compare different images and/or different areas of the images. Moreover, this problem has also been observed when comparing different morphologies on a given length scale.[36] With the aim of determining if this problem was manifested in our samples, other formalisms based on the power spectral density (PSD) were applied with the aid of Gwyddion v.2.23 (open-source software)[35] to calculate the roughness and D_F (details in the Supporting Information).

2.6. Detrended Fluctuation Analysis (DFA). The height data series obtained from AFM studies on LB films were submitted to fractal analysis, as described in detail elsewhere.[37,38] For DFA purposes, data were obtained from the height fluctuations along lines crossing the AFM image of the LB sample, in several directions (Figure 2). This method, based on the Hurst exponent, has been introduced by Peng et al.[39] to analyze the organization of DNA sequences. Since then, it has been used to analyze series data of many different origins.[40] The advantage of DFA compared to other fluctuation analyses is its applicability to nonstationary data series. Briefly, in DFA a self-similarity parameter (α value) was calculated as the slope of a log−log plot of fluctuation ($\log F(n)$) vs windows size ($\log n$) for n within the range of 4 ($\log n = 0.6$) to 160 ($\log n = 2.2$) data points, where $F(n)$ (eq 2) is the root square of the mean quadratic deviations of each y_i value with respect to the regression line $\hat{y}_{i,k}$ within the corresponding window (k).

$$F(n) = \sqrt{\frac{\sum_{i=1}^{N} [(y_i - \hat{y}_{i,k}]^2}{N}} \tag{2}$$

The α value provides a measure of the roughness of the original data series: the larger the value of α, the smoother the data series.[41] Also, in DFA the α exponent is inversely related to a typical fractal dimension, so in this case, the value increases with increasing regularity (or decreasing complexity) in the data series.[42] Different values of the α exponent signify different levels of spatial correlation in fluctuation on different scales. For data series of processes where fluctuations are negatively correlated ("antipersistent" noise), we have $0 < \alpha < 0.5$. For data series with consecutive values generated by statistically independent processes with finite variances, $\alpha = 0.5$ (uncorrelated or "white" noise); in this case the data has short-range correlations (i.e., the correlations decay exponentially). $0.5 < \alpha < 1$ corresponds to processes where fluctuations in subsequent values are positively (long-range) correlated ("persistent" noise), and correlations decay as a power law, meaning that ongoing behavior is influenced by what has occurred in the previous positions.[43] $\alpha = 1$ corresponds to power spectral $1/f$ noise that is typical of systems near self-organized critical states.[44] Values of α in the range of $1 < \alpha < 1.5$ correspond to integrated negatively correlated (antipersistent) noise, where $\alpha = 1.5$ ("brown" noise) corresponds to integrated independent increments of white noise.[45] The presence of self-similarity in raw data and its disappearance after randomization are illustrated in Figure S3 (Supporting Information).

2.7. SDS Polyacryamide Gel Electrophoresis (SDS-PAGE). The protein compositions of the different SM samples (SM suspension, SM monolayers, and transferred SM to alkylated glasses) were compared by means of Laemmli SDS-PAGE[46] using 10 and 4% poliacrylamide as running and stacking gels, respectively.

In the case of LB films, the transferred SM was washed off of the glass substrates with 0.3 w/v % SDS and sonicated for 5 min to extract SM components. The excess SDS was removed by dialysis against bidistilled water through a cellulose membrane (12 kDa cutoff). Samples were lyophilized, kept at −20 °C, resuspended in sample buffer, and submitted to SDS-PAGE as described above. Band patterns were analyzed by densitometry using free ImageJ 1.48 v software (Wyne Rasband, NIH, USA). (See details in the Supporting Information).

2.8. Radioligand Binding Assay. The binding assay was performed essentially as described previously.[47] BZDs [^{3}H]FNZ and DZ were used as label and nonlabel ligands, respectively.

Two sets of samples were prepared, one in the presence (NB) and the other in the absence (TB) of DZ, which allowed the measurement of nonspecific (NB) and total (TB) radiolabeled ligand bound to the membrane, respectively. Specific binding (B) was calculated as the difference between TB and NB.

2.8.1. [^{3}H]FNZ Binding to the SM Suspension. The incubation system (230 μL final volume) contained SM (0.25 mg/mL final total protein concentration) dispersed in 100 mM NaCl−50 mM Tris-HCl pH 7.4 buffer and 0.5−12 nM [^{3}H]FNZ (minimum specific activity 81.4 Ci/mmol). Then, 20 μL of the same buffer, containing (NB sample set) or not containing (TB sample set) 106 μM DZ was added to give a 9.4 μM DZ final concentration.

Samples were incubated at 4 °C in the dark for 1 h and then filtered through Whatman GF/B type SS filters with a Brandel automatic filtration apparatus (Brandel, Gaithersburg, MD, USA). Filters were rinsed and dried in air.

2.8.2. [^{3}H]FNZ Binding to SM Langmuir−Blodgett Films. For the radioligand binding assay to LB_{1c}, variable volumes of [^{3}H]-FNZ solutions (180 or 360 nM) were added to the bath water containing LB_{1c} to obtain 0.2−50 nM final ligand concentrations. Then, diazepam (5μL) was added only to NB samples to reach a 9.24 μM DZ final concentration in the total volume (~0.18 mL).

For the radioligand binding assay to LB_{2c}, samples were placed in tubes containing [^{3}H]-FNZ at concentrations ranging from 1 to 60 nM, 20 μL of DZ (3.5 mM, only in NB samples), and enough bidistilled water to reach a 0.75 mL total volume.

Samples, both LB_{1c} and LB_{2c}, were incubated at 4 °C in the dark for 1 h. Afterwards, to check the actual [^{3}H]FNZ concentration, three 5 μL aliquots were taken from the supernatant (representing the free [^{3}H]FNZ fraction) which was then eliminated using a Pasteur pipet connected to a vacuum pump. LBs were separately placed in clean plastic vials for radioactivity measurement. Determinations were performed in triplicate.

2.8.3. Radioactivity Measurement. Filters (SM samples) or glasses (LB_{1c} and LB_{2c} films) placed in vials containing 2.5 mL of scintillation liquid (25%V/V Triton X-100, 0.3% W/V diphenyloxazole in toluene) were incubated overnight, and then the radioactivity was measured with a Rackbeta 1214 scintillation spectrometer (Pharmacia-LKB, Finland) at 60% efficiency for tritium.

2.9. Kinetic Parameter Determination. Equation 3 was fitted to the saturation curves (specific binding vs free [^{3}H]FNZ concentration), by a nonlinear regression analysis performed by a computer-aided least-squares method[48]

$$B = \frac{B_{max} F}{K_d + F} \tag{3}$$

where F is the free [^{3}H]FNZ concentration and B and B_{max} are the specific binding activities, ligand-concentration-dependent and maximal, respectively (both of them normalized per unit of protein mass). K_d is the equilibrium dissociation constant.

2.10. Protein Quantitation. The protein concentration was determined according to the Lowry method.[49] In the case of LB films, before protein quantification the film was washed out of the alkylated glass with 1% SDS (0.05 mL) and sonicated for 5 min to extract SM components. A blank sample contained water or membrane-free SDS solution (details in the Supporting Information).

2.11. Statistical Analysis. For comparison, a two-tailed student's t test for independent samples or a one-way analysis of variance (ANOVA), according to the experiment, was conducted.[50] Linear regression analysis was done by the least-squares method.

3. RESULTS

3.1. LB Film Topography. AFM was performed for the purpose of confirming the monolayer transference from the air−water interface to the solid substrate as well as to obtain information about the film surface organization and topography

DOI: 10.1021/la5042986
Langmuir XXXX, XXX, XXX−XXX

of the LB film obtained. AFM images showed a homogeneous aspect of the membrane-free alkylated glass (control sample, CON_{glass}) (Figure 1a) while LB films obtained at 15 mN/m

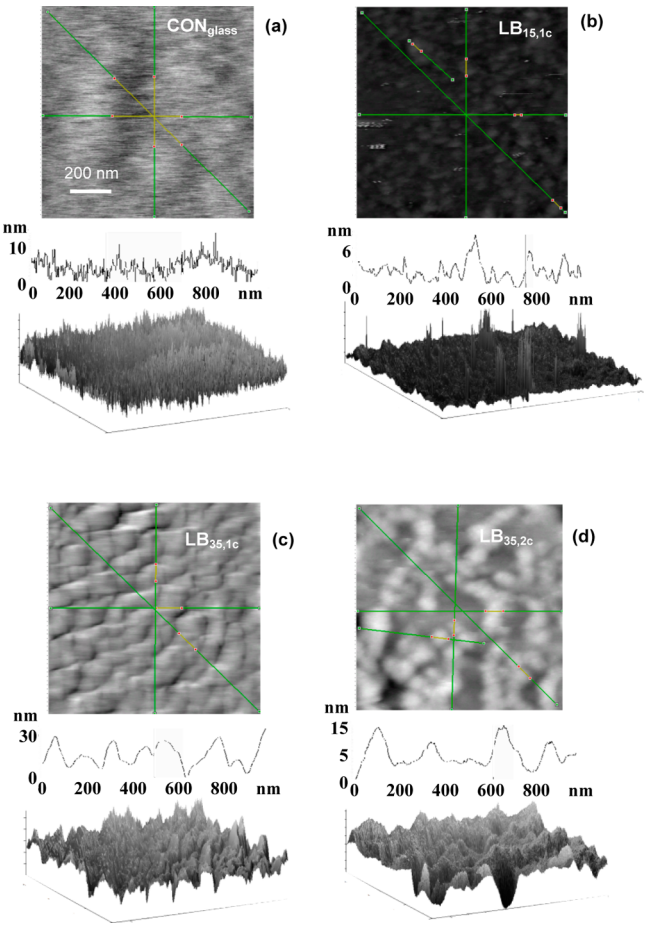

Figure 1. AFM images of sinaptosomal membrane LB films. (a) CON_{glass}: clean alkylated glass (without SM). (b) $LB_{15/1c}$, CON_{glass} coated with one layer of SM packed at 15 mN/m. (c and d) CON_{glass} coated with one ($LB_{35/1c}$) or two ($LB_{35/2c}$) layers of SM packed at 35 mN/m. Each panel includes a 2D AFM image and a height fluctuation via the diagonal line outlined in the AFM images and 3D reconstruction of the AFM image of the same sample.

(LB_{15}) as well as at 35 mN/m with one or two transferred layers ($LB_{35,1c}$ or $LB_{35,2c}$, respectively) adopted the thin film organization with significant lateral anisotropy (Figure 1b–d) .

An analysis of fluctuation vs position allows us to calculate the following parameters: fractal dimension (D_F), average roughness (R_a) (eq 1) of the images,[51] wide frequency height distribution peak ($\bar{H}$), maximum height (H_m), and the most frequent height (H^+) (Table 1).

On the 1 μm scale, the R_a values for all LB films were similar to that of CON_{glass} except for $LB_{35,1c}$, which exhibited a value that was significantly greater. The same behavior was observed with $\bar{H}$ and H^+ values. On the other hand, the H_m values of all types of LB samples tested were greater than that of the CON_{glass}.

The height pattern along a line drawn through the AFM image (Figure 2a–d) within the most frequent heights (H^+) of the topographic structures present in the films varied between 7 and 50 nm (Table 1). This allowed us to discard the possibility of vesiculization of the SM monolayer components during the

Table 1. Topographic Analysis of the AFM Images (Scale = 1 μm)

	R_a (Å)	H_m (nm)	H^+ (nm)	$\bar{H}$ (nm)	D_F
CON_{glass}	19.2	21.2	12 (0.70)	5	2.47
$LB_{15,1c}$	15.8	53.4	7 (0.80)	4	2.32
$LB_{35,1c}$	**68.4**	85.6	50 (0.70)	20	**2.17**
$LB_{35,2c}$	32.2	30.8	18 (0.50)	14	2.29

D_F, fractal dimension; R_a, roughness; H_m, maximal height; H^+, more likely height; $\bar{H}$, average height. Numbers between brackets represent the probability (β) of finding H^+.

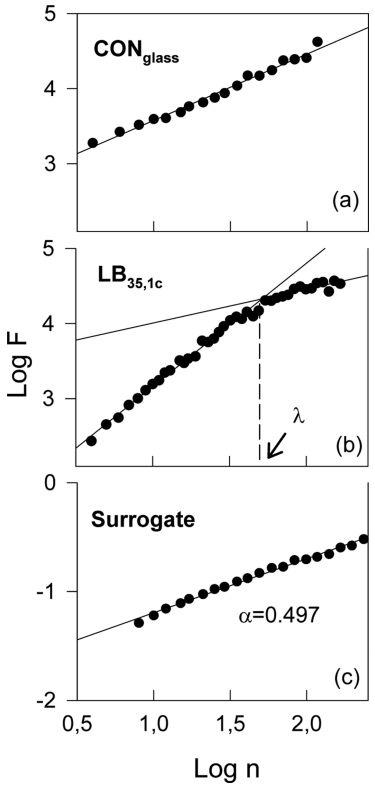

Figure 2. DFA analysis of AFM images. Typical log–log plots of the heights fluctuation as a function of the window size (log $F(n)$ versus log n) (eq 2) using data taken from the diagonal line of AFM images shown in Figure 1. (a) CON_{glass}, (b) $LB_{35,1c}$, and (c) result from the randomization of values in (b).

transference process. Since the size of synaptosomal vesicles as determined trough transmition electron microscopy has been reported to be approximately 240 nm,[52] it can be accepted that the membrane transferred to the alkylated glass conserved its planar geometry. Finally, the D_F value did not allow us to discriminate differences between CON_{glass} and LB films, except for $LB_{35,1c}$, which exhibited the lowest magnitude (Table 1). Note that this fact is reinforced by the results obtained through the application of the PDS algorithm of Gwyddion (Table S2 in the Supporting Information).

The height fluctuation (eq 2) along three lines drawn up in several directions on each AFM image (Figure 1) was plotted as a function of the window size in a log–log plot (Figure 2), and the α autosimilarity parameter was obtained from the slope.

Except for CON_{glass} (Figure 2), all samples exhibited bimodal behavior (see Figure 2b as an example) which became unimodal with $\alpha \approx 0.5$ typical of white noise after data randomization (Figure 2c). The values of α as well as those of n

DOI: 10.1021/la5042986
Langmuir XXXX, XXX, XXX–XXX

Table 2. Detrended Fluctuation Analysis of the LB Films of Synaptosomal Membranes[a]

			autocorrelation length (λ)	
	α_1	α_2	log n	(nm)
CON_{glass}	1.046 ± 0.132			
$LB_{15,1c}$	1.453 ± 0.085	0.735 ± 0.073	1.6 ± 0.1	87.04 ± 29.47
$LB_{35,1c}$	1.574 ± 0.087	0.695 ± 0.141	1.73 ± 0.03	107.43 ± 8.69
$LB_{35,2c}$	1.808 ± 0.111	1.438 ± 0.097	1.65 ± 0.22	115.80 ± 63.44

[a]Values correspond to the mean ± SEM of triplicates; α = self-similarity parameter.

at the inflection point (λ) were also registered (Table 2). Parameter λ indicated the scale size at which occurred a qualitative change in the α value from Brownian-type noise ($\alpha > 1$) to a long-range autocorrelation regime ($0.5 > \alpha < 1$) when the alkylated glass was covered with a stable membrane film ($LB_{15,1c}$–$LB_{35,2c}$). The CON_{glass} sample showed a single α value not significantly different from unity (characteristic of $1/f$ noise). $LB_{15,1c}$ films exhibited a high dispersion in the α values for the different directions (height SEM). This suggests a strong irregularity that may reflect a low molecular cohesion in this film organization. In spite of this, the height fluctuation behavior of $LB_{35,1c}$- and $LB_{35,2c}$-coated substrates was significantly different from an aleatory distribution as revealed after DFA of the same height data that was previously randomized (Figure 2c).

3.2. LB Protein Composition. SDS-PAGE was carried out to evaluate possible changes in the film protein composition after the packing of the SM Langmuir film (LF) and after the transference of the LF to the alkylated glass to prepare the LB film, with respect to the SM original suspension (Figure 3, right panels). Membrane samples were recovered from LB films ($LB_{15,1c}$, $LB_{35,1c}$, and $LB_{35,2c}$), and the material at the air–water interface was recovered by suction from the LF packed at 35 mN/m. An aqueous SM suspension was used as a control sample, and the protein band profile was evaluated through a densitometric analysis of stained SDS-PAGE gels (Figure 3, left panels). SDS-PAGE suggests that neither the material extracted from LB films nor the membranes recovered by suction from the air–water interface exhibited significant changes within the region where we expect to find the $GABA_A$-R subunits (e.g., the MW of the α_2 subunit is 53 000). A slight displacement of the whole band profile in LBs samples toward apparently higher MW compared to bands in SM (Figure 3, left panels) can be explained as a disturbance induced by excess SDS, used to detach proteins from the substrate, that could not be exhaustively eliminated (Figures S5 and S6 in the Supporting Information). In addition, the absence of bands in the region of low-MW proteins in LB samples may be related to the fact that the dialysis membrane might not have retained low-MW proteins which, as components of mixed SDS–lipid–protein micelles, may have crossed the dialysis membrane pore.

3.3. [^{3}H]-FNZ Binding to LB Films. Two methods were applied for the alkylation of glass substrates for LB film preparation which used either hexadecane or toluene to dissolve the alkylating agent. It was reported that a higher molecular density of hydrocarbon chains covalently bound to the glass surface can be achieved using toluene as the solvent.[32] The capacity of [^{3}H]FNZ to interact nonspecifically with the surface of the alkylated glass was tested in both alkylated and nonalkylated (clean) glasses (Figure 4). Nonspecific [^{3}H]FNZ binding was higher to glasses covered with a lower alkyl chain density (using hexadecane). This agrees with previous results indicating that the FNZ partition coefficient correlated inversely with the molecular membrane packing (ref 26 and refs therein). Nonalkylated glass, being hydrophilic, exhibited the lowest [^{3}H]FNZ nonspecific binding (5 or 7 times lower than with alkylated glasses). On the other hand, in LB films prepared on a glass covered with a high hydrocarbon chain density (using toluene for alkylation) the SM transference was less effective and the specific [^{3}H]FNZ binding was negligible. Consequently, hexadecane was chosen as a solvent for the alkylation process even if it produced higher nonspecific binding.

To keep the number of chemical species in the system at a minimum, the subphase used to prepare the SM monolayers was bidistilled water. Thus, this was the medium in which all subsequent binding experiments were carried out.

The saturation binding curve of [^{3}H]FNZ was tested with SM vesicles dispersed in water as well as in buffer (used as a control) (Figure 5a). The B_{max} in water was significantly smaller than that observed in buffer; nevertheless, the affinity was noticeably greater (Table 3). Then, the suspension of SM in water was the system taken as a reference to compare with LB samples.

Figure 5b–d shows the effect of the molecular membrane packing on the [^{3}H]FNZ binding kinetics in LB films of SM. Only in the case of [^{3}H]FNZ binding to $LB_{35/2c}$, samples TB and NB obtained were superimposed and prevent the B calculation (Figure 5b). At low membrane packing (15 mN/m), the specific binding increased as a function of [^{3}H]FNZ concentration, but this curve did not reach saturation (Figure 5c). The [^{3}H]FNZ binding kinetics changed qualitatively and quantitatively when the molecular packing increased from 15 to 35 mN/m, and the curve obtained for [^{3}H]FNZ binding to the $LB_{35/1c}$ sample followed sigmoidal behavior (Figure 5d). Table 3 summarizes the values obtained for the kinetic parameters in each case.

4. DISCUSSION

In the present work we applied the working experience of our laboratory in different biomembrane models to prepare $GABA_A$-R inserted in a molecular environment close to that of a natural membrane with the aim of developing a membrane-based biosensor for benzodiazepines and other $GABA_A$-R ligands. Therefore, we chose the LB film model, and after demonstrating its successful preparation (Figures1 and 2), we studied its binding activity.

The molecular immobilization and the molecular packing modified both the maximal binding of [^{3}H]FNZ and the binding affinity, K_d. As summarized in Table 3, the affinity followed the trend $LB_{15,1c} < LB_{35,1c} <$ vesicles. On the other hand, the B_{max} value was greater in LB films ($LB_{15,1c} > LB_{35,1c}$) with respect to vesicles.

The increase in B_{max} values suggests a better accessibility of FNZ to their binding sites in the receptor. On the one hand,

DOI: 10.1021/la5042986
Langmuir XXXX, XXX, XXX–XXX

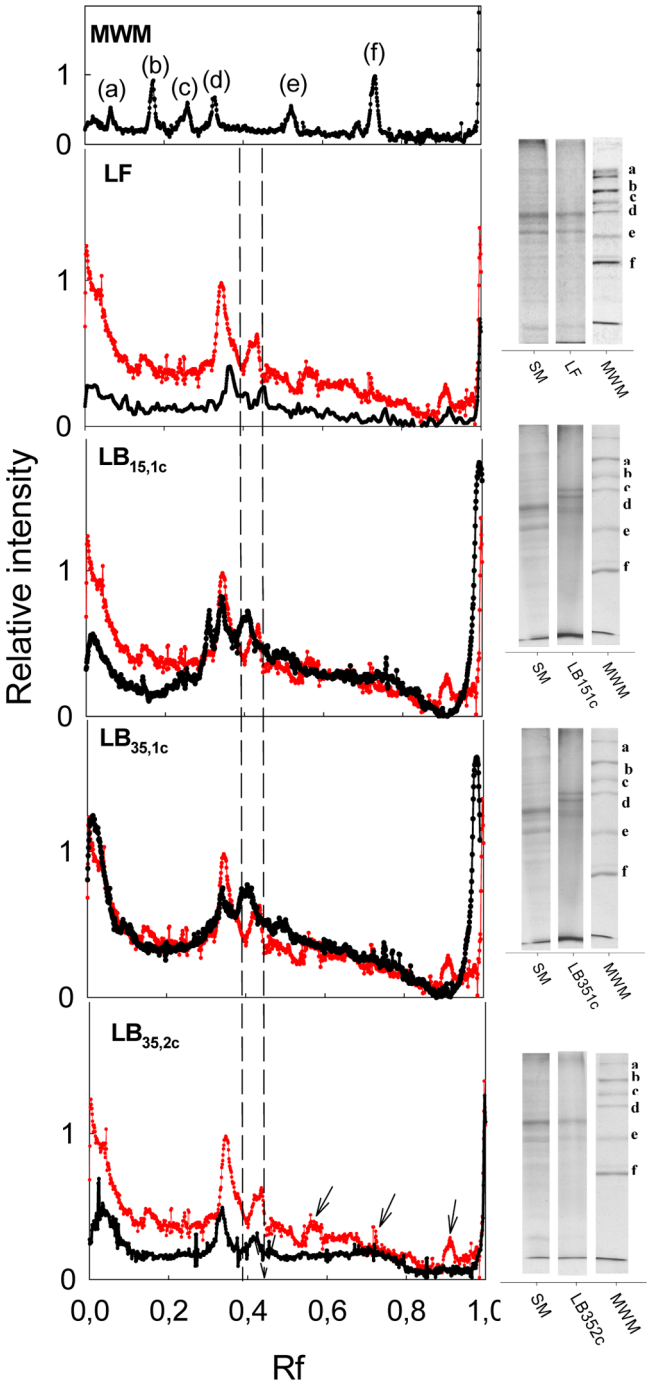

Figure 3. SDS-PAGES of sinaptosomal membranes recovered from Langmuir and LB films and their densitometry band profile. From top to bottom: (left panels) densitometry of molecular weight markers, LF, $LB_{15/1c}$, $LB_{35/1c}$, and $LB_{35/2c}$ band profiles (black lines) superimposed on the densitometric profile of SM (red lines). Arrows point to small proteins possibly not retained by the dialysis membrane (see the text). (Right panels) Commassie blue-stained SDS-PAGE of LF, $LB_{15/1c}$, $LB_{35/1c}$, and $LB_{35/2c}$ samples flanked by MWM and SM as references. Dashed lines along desitometric profiles mark the expected position of the $GABA_A$-R α subunit band. MWM bands from top to bottom are Miosine mouse muscle (a), β-galactosidase of *E. coli* (b), bovine lactoferrine (c), bovine seroalbumin (d), an intracellular fragment of PTP-IA-2B (e), and β-lactamase of *B. licheniformis* (f). Molecular weights: 205 000, 116 000, 90 000, 66 000, 44 300, and 32 000, respectively. Dotted lines in densitometry profiles mark the expected position of the $GABA_A$-R α subunit band.

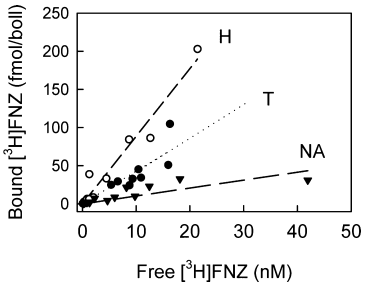

Figure 4. Nonspecific binding of [^{3}H]FNZ. NA, nonalkylated clean glass; H and T, glasses alkylated with OTS dissolved in hexadecane and in toluene, respectively.

this could be related to the loss of nonreceptor proteins that occurred in SM but not in LB (Figure 3) or to fractal kinetics where the reaction order does not reflect the reaction molecularity but the fractal dimension of the space where the reaction (in this case, [^{3}H]FNZ binding) is occurring.[53] This fractal kinetic model as well as an allosteric model might explain the sigmoidal shape of the binding curve. The latter can reflect the degree of interconnection between the receptor subunits. However, since the membrane organization in LB differed from that in SM, the coupling between the receptor sites could be affected and the behavior may not be necessarily similar to that observed in the well-known vesicle system.

From B_{max} values (Table 3) it can be estimated that the distance between two binding sites in the LB films would be around 10 and 20 nm in $LB_{15,1c}$ and $LB_{35,1c}$ samples, respectively. Although this would seem to be too close if compared to the diameter of the crystal structure of the human β3-homopentamer $GABA_A$-R,[54] it seems reasonable if compared to 44 and 34 nm, which can be calculated from the density of $GABA_A$ receptors at inhibitory synapses on somata (510 receptors/μm^2) and axon initial segments (850 receptors/μm^2) as reported by Nusser et al.[55] in a study performed with hippocampal granule cells evaluated through immunogold localization associated with transmission electron microscopy. However, contrary to what would be expected from a simple compaction effect, the binding surface density decreases with surface pressure. Additionally, the K_d/B_{max} relationship found with $LB_{15,1c}$ and $LB_{35,1c}$ follows the tendency of lower affinity/higher capacity typically found in membrane-bound receptors. This suggests a change in the characteristics of the binding sites accessible at each surface pressure.

Structural portions within each receptor subunit located near the membrane interface appear to be involved in gating receptor transitions.[56−59] Some authors have explored the functional role of the β-10 strand (pre-M1segment) that connects the extracellular domain to the transmembrane domain and have concluded that it is a key functional component in the activation of the $GABA_A$-R.[60] On the other hand, a mechanism whereby adjacent $GABA_A$-R components interact via their amphipathic intracelular helix γ2 subunits, altering ion permeation through each channel, has been proposed.[61] Then, the topology of the $GABA_A$-R-containing film could be affecting this protein−protein interaction.

In general, the difference found in the FNZ binding, comparing different LB films, agrees with the differences found in the PSD and the DFA analyses. The structure of $LB_{35,2c}$ differs from that of one-layer films ($LB_{15,1c}$ and $LB_{35,1c}$), possibly due to molecular reorganizations occurring during the transference of the second layer (the membrane contacts the

DOI: 10.1021/la5042986
Langmuir XXXX, XXX, XXX−XXX

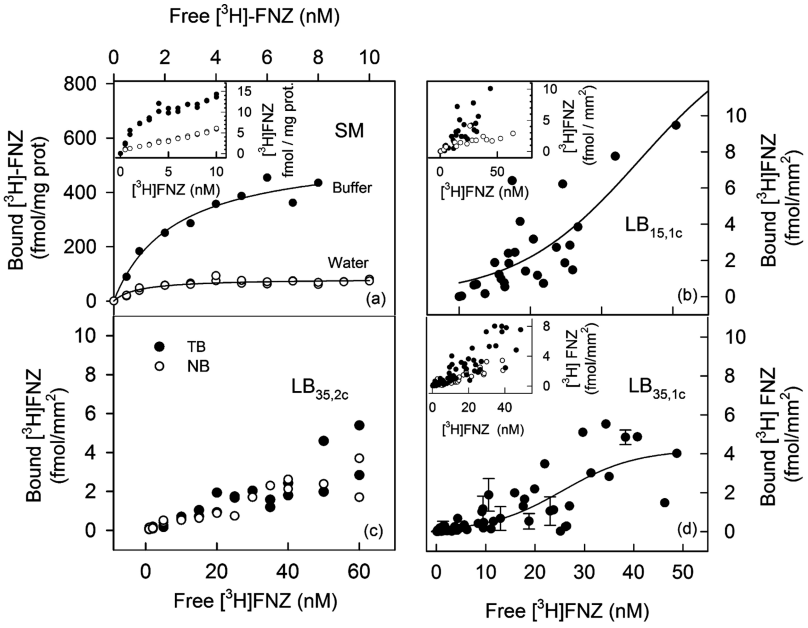

Figure 5. Binding of [^{3}H]FNZ to sinaptosomal membranes. (a) Specific binding of [^{3}H]FNZ to SM resuspended in water or in buffer. (b) Total binding (TB, ●) and nonspecific binding (NB, ○) of [^{3}H]FNZ to $LB_{35/2c}$. (c) Specific binding of [^{3}H]FNZ to $LB_{15/1c}$. (d) Specific binding of [^{3}H]FNZ to $LB_{35/1c}$. The inset shows the TB (●) and NB (○) binding curves in each case. $LB_{15/1c}$, $LB_{35/1c}$, and $LB_{35/2c}$: alkylated glass coated with one (1c) or two (2c) layers of SM monolayers packed at 15 or at 35 mN/m.

Table 3. Kinetics Parameters of [^{3}H]FNZ Binding to the $GABA_A$-R Present in the LB Films and in the Aqueous SM Suspension[a]

		B_{max}	
sample	K_D (nM)	(fmol/mg prot)	(fmol/mm^2)
SM_{buffer}	2.3 ± 0.6	555 ±50	
SM_{water}	0.95 ± 0.23	83 ± 4	
$LB_{15,1c}$	51 ± 27		15 ± 1[b]
$LB_{35,1c}$	26 ± 4		4.2 ± 0.7[c]
$LB_{35,2c}$			

[a]Values correspond to the mean ± SEM. Specific binding was negligible in $LB_{35,2c}$ samples. [b]110 nm^2/binding site. [c]392 nm^2/binding site.

air, which may induce a molecular rearrangement). In addition, the smaller molecular cohesion in $LB_{15,1c}$ could explain the different shape of its binding curve.

Finally, $LB_{35,1c}$ films (sigmoidal binding curve) have the smallest values for both D_F obtained through PSD and the self-similarity parameter (α) obtained from DFA. This could be interpreted as a more efficient transference of the monolayer or as a more homogeneous monolayer in the plane of the LB film. Additionally, all of the algorithms that were applied consistently showed that $LB_{35,c}$ exhibited the greatest roughness and heights (H_m, H^+, and $\bar{H}$), suggesting a lower molecular tilt associated with the tighter molecular packing and global film organization.

Mechanosensitive channels comprise a group of channels gated by a mechanical force that is generally generated by membrane stretching. They are of special interest because most of them are activated by the membrane tension and report the physical contact with lipids.[62] For example, while the NMDA receptors are primarily ligand-gated channels, they are also sensitive to voltage and to mechanical forces: at a given voltage and in the presence of fixed concentrations of glutamate and glycine, the membrane stretch increases and membrane compression decreases their probability of opening.[19,63]

5. CONCLUSIONS

Until now, neither the relationship between topology and ligand binding in $GABA_A$-R nor the separation of topological effects from those induced by the molecular density has been studied. The differences found in the FNZ binding seem to be related not only to the degree of membrane packing but also to the way in which the membrane components are organized on the solid support once transferred. Also, our results might be suggesting an underlying mechanosensitivity, providing a possible explanation and the connection observed between the binding kinetics and the film topological organization.

Moreover, these stable bioactive surfaces may serve as platforms for the study of relevant membrane receptors for other neuroactive compounds.

■ ASSOCIATED CONTENT

Supporting Information

Enlarged π–A compression isotherm of the SM monolayer, transfer parameters recorded during LB film formation, detailed description of detrended fluctuation analysis (DFA), SDS polyacryamide gel electrophoresis (SDS-PAGE), and protein quantification. Results for the effect of high SDS concentration in the band pattern of SDS-PAGE. This material is available free of charge via the Internet at http://pubs.acs.org.

■ AUTHOR INFORMATION

Corresponding Author

*Tel: +54-351-5353800 (29777). Fax: +54-351-4334139. E-mail: mperillo@efn.uncor.edu.

Notes

The authors declare no competing financial interest.

DOI: 10.1021/la5042986
Langmuir XXXX, XXX, XXX−XXX

■ ACKNOWLEDGMENTS

The present work was partially financed by grants from Foncyt, SECyT-Universidad Nacional de Córdoba, and CONICET. P.D.C. holds a postdoctoral fellowship from CONICET. M.A.P. and A.V.T. are career investigators of the latter institution.

■ ABBREVIATIONS

AFM, atomic force microscopy; B_{max}, maximal binding; DFA, detrended fluctuation analysis; DZ, diazepam; FNZ, flunitrazepam; CON_{glass}, alkylated glass free of the LB film used as a control sample; GABA, γ-amino butyric acid; K_d, equilibrium dissociation constant; LB, Langmuir−Blodgett; LF, Langmuir film; $GABA_A$-R, type A GABA receptor; NB, nonspecific binding; OTS, octadecyl trichlorosilane; SDS, sodium dodecylsulfate; SDS-PAGE, polyacrylamide gel electrophoresis in the presence of SDS; SEM, standard error of the mean; SM, synaptosomal membranes; TB, total binding

■ REFERENCES

(1) Gaines, G. *Insoluble Monolayers at Liquid−Gas Interfaces*; Interscience Publishers: New York, 1966.
(2) Zasadzinski, J. A.; Viswanathan, R.; Madsen, L.; Garnaes, J.; Schwartz, D. K. Langmuir-Blodgett Films. *Science* **1994**, *263*, 1726−1733.
(3) Chovelon, J. M.; Provence, M.; Jaffrezic-Renault, N.; Alexandre, S.; Valleton, J. M. Transfer of Mixed Protein−Fatty Acid Lb Films onto Si/SiO_2 Substrates. Influence of the Surface Free Energy. *Mater. Sci. Eng. C* **2002**, *22*, 79−85.
(4) Ariga, K.; Yamauchi, Y.; Mori, T.; Hill, J. P. 25th Anniversary Article: What Can Be Done with the Langmuir-Blodgett Method? Recent Developments and Its Critical Role in Materials Science. *Adv. Mater.* **2013**, *25*, 6477−6512.
(5) Whitesides, G. M.; Mathias, J. P.; Seto, C. T. Molecular Self-Assembly and Nanochemistry: A Chemical Strategy for the Synthesis of Nanostructures. *Science* **1991**, *254*, 1312−1319.
(6) Davis, F.; Higson, S. P. Structured Thin Films as Functional Components within Biosensors. *Biosens. Bioelectron.* **2005**, *21*, 1−20.
(7) Girard-Egrot, A. P.; Godoy, S.; Blum, L. J. Enzyme Association with Lipidic Langmuir-Blodgett Films: Interests and Applications in Nanobioscience. *Adv. Colloid Interface Sci.* **2005**, *116*, 205−225.
(8) Clop, E. M.; Clop, P. D.; Sanchez, J. M.; Perillo, M. A. Molecular Packing Tunes the Activity of Kluyveromyces Lactis Beta-Galactosidase Incorporated in Langmuir-Blodgett Films. *Langmuir* **2008**, *24*, 10950−10960.
(9) Patching, S. G. Surface Plasmon Resonance Spectroscopy for Characterisation of Membrane Protein−Ligand Interactions and Its Potential for Drug Discovery. *Biochim. Biophys. Acta* **2014**, *1838*, 43−55.
(10) Seeger, C.; Christopeit, T.; Fuchs, K.; Grote, K.; Sieghart, W.; Danielson, U. H. Histaminergic Pharmacology of Homo-Oligomeric B3 G-Aminobutyric Acid Type a Receptors Characterized by Surface Plasmon Resonance Biosensor Technology. *Biochem. Pharmacol.* **2012**, *84*, 341−351.
(11) Cantor, R. S. Solute Modulation of Conformational Equilibria in Intrinsic Membrane Proteins: Apparent "Cooperativity" Without Binding. *Biophys. J.* **1999**, *77*, 2643−2647.
(12) Perillo, M. A.; Garcia, D. A. Flunitrazepam Induces Geometrical Changes at the Lipid-Water Interface. *Colloids Surf., B* **2001**, *20*, 63−72.
(13) Turina, A. V.; Perillo, M. A. Monoterpenes Affect Chlorodiazepoxide-Micelle Interaction through Micellar Dipole Potential Modifications. *Biochim. Biophys. Acta* **2003**, *1616*, 112−120.
(14) Garcia, D. A.; Perillo, M. A. Supramolecular Events Modulate Flunitrazepam Partitioning into Natural and Model Membranes. *Colloids Surf., B* **1997**, *9*, 49−57.
(15) Honig, B. H.; Hubbell, W. L.; Flewelling, R. F. Electrostatic Interactions in Membranes and Proteins. *Annu. Rev. Biophys. Biophys. Chem.* **1986**, *15*, 163−193.
(16) Cladera, J.; O'Shea, P. Intramembrane Molecular Dipoles Affect the Membrane Insertion and Folding of a Model Amphiphilic Peptide. *Biophys. J.* **1998**, *74*, 2434−2442.
(17) Maggio, B. Modulation of Phospholipase A2 by Electrostatic Fields and Dipole Potential of Glycosphingolipids in Monolayers. *J. Lipid Res.* **1999**, *40*, 930−939.
(18) Del Boca, M.; Caputto, B. L.; Maggio, B.; Borioli, G. A. C-Jun Interacts with Phospholipids and C-Fos at the Interface. *J. Colloid Interface Sci.* **2005**, *287*, 80−84.
(19) Paoletti, P.; Ascher, P. Mechanosensitivity of Nmda Receptors in Cultured Mouse Central Neurons. *Neuron* **1994**, *13*, 645−655.
(20) Lipowski, R. Domains and Rafts in Membranes - Hidden Dimensions of Self-Organization. *J. Biol. Phys.* **2002**, *28*, 195−210.
(21) Yoshimura, K.; Sokabe, M. Mechanosensitivity of Ion Channels Based on Protein-Lipid Interactions. *J. R. Soc. Interface* **2010**, *10*, S307−S320.
(22) Mehta, A. K.; Ticku, M. K. An Update on Gabaa Receptors. *Brain Res. Rev.* **1999**, *29*, 196−217.
(23) Perillo, M. A.; Garcia, D. A.; Arce, A. Partitioning of 1,4-Benzodiazepines into Natural Membranes. *Mol. Membr. Biol.* **1995**, *12*, 217−224.
(24) Garcia, D. A.; Perillo, M. A. Partitioning of Flunitrazepam into Model Membranes Studied by Temperature Controlled Gel Filtration Chromatography. *Biomed. Chromatogr.* **1997**, *11*, 343−347.
(25) Garcia, D. A.; Perillo, M. A. Benzodiazepine Localisation at the Lipid-Water Interface: Effect of Membrane Composition and Drug Chemical Structure. *Biochim. Biophys. Acta* **1999**, *1418*, 221−231.
(26) Garcia, D. A.; Perillo, M. A. Flunitrazepam-Membrane Non-Specific Binding and Unbinding: Two Pathways with Different Energy Barriers. *Biophys. Chem.* **2002**, *95*, 157−164.
(27) Perillo, M. A.; Arce, A. Determination of the Membrane-Buffer Partition Coefficient of Flunitrazepam, a Lipophilic Drug. *J. Neurosci. Methods* **1991**, *36*, 203−208.
(28) Perillo, M. A.; Polo, A.; Guidotti, A.; Costa, E.; Maggio, B. Molecular Parameters of Semisynthetic Derivatives of Gangliosides and Sphingosine in Monolayers at the Air-Water Interface. *Chem. Phys. Lipids* **1993**, *65*, 225−238.
(29) Vargaftik, N. B.; Volkov, B. N.; Voljk, L. D. International Tables of the Surface Tension of Water. *J. Phys. Chem. Ref. Data* **1983**, *12*, 817−820.
(30) Verger, R.; Pattus, F. Spreading of Membranes at the Air/Water Interface. *Chem. Phys. Lipids* **1976**, *16*, 285−291.
(31) Oliveira, R. G.; Calderon, R. O.; Maggio, B. Surface Behavior of Myelin Monolayers. *Biochim. Biophys. Acta* **1998**, *1370*, 127−137.
(32) McGovern, M. E.; Kallury, K. M. R.; Thompson, M. Role of Solvent on the Silanization of Glass with Octadecyltrichlorosilane. *Langmuir* **1994**, *10*, 3607−3614.
(33) von Tscharner, V.; McConnell, H. M. Physical Properties of Lipid Monolayers on Alkylated Planar Glass Surfaces. *Biophys. J.* **1981**, *36*, 421−427.
(34) Rieu, J. P.; Ronzon, F.; Place, C.; Dekkiche, F.; Cross, B.; Roux, B. Insertion of Gpi-Anchored Alkaline Phosphatase into Supported Membranes: A Combined Afm and Fluorescence Microscopy Study. *Acta Biochim. Pol.* **2004**, *51*, 189−197.
(35) Nečas, D.; Klapetek, P. Gwyddion: An Open-Source Software for Spm Data Analysis. *Cent. Eur. J. Phys.* **2012**, *10*, 181−188.
(36) Stefanutti, E.; Papacci, F.; Sennato, S.; Bombelli, C.; Viola, I.; Bonincontro, A.; Bordi, F.; Mancini, G.; Gigli, G.; Risuleo, G. Cationic Liposomes Formulated with Dmpc and a Gemini Surfactant Traverse the Cell Membrane without Causing a Significant Bio-Damage. *Biochim. Biophys. Acta* **2014**, *1838*, 2646−2655.
(37) Kembro, J. M.; Satterlee, D. G.; Schmidt, J. B.; Perillo, M. A.; Marin, R. H. Open-Field Temporal Pattern of Ambulation in Japanese Quail Genetically Selected for Contrasting Adrenocortical Responsiveness to Brief Manual Restraint. *Poult. Sci.* **2008**, *87*, 2186−2195.

DOI: 10.1021/la5042986
Langmuir XXXX, XXX, XXX−XXX

(38) Kembro, J. M.; Perillo, M. A.; Marin, R. H. Análisis De Fluctuación Con Eliminación De Tendencias En Estudios De Comportamiento Animal: Los Efectos De La Inactividad Inducida Por Estrés. *Acta Acad Nac. Cienc. (Córdoba)* **2008**, *XIV*, 108−116.
(39) Peng, C. K.; Buldyrev, S. V.; Havlin, S.; Simons, M.; Stanley, H. E.; Goldberger, A. L. Mosaic Organization of DNA Nucleotides. *Phys. Rev. E: Stat., Nonlinear, Soft Matter Phys.* **1994**, *49*, 1685−1689.
(40) Corvalán, N. A.; Kembro, J. M.; Clop, P. D.; Perillo, M. A. Cholesterol Favors the Emergence of a Long-Range Autocorrelated Fluctuation Pattern in Voltage-Induced Ionic Currents through Lipid Bilayers. *Biochim. Biophys. Acta, Biomembr.* **2013**, *1828*, 1754−1764.
(41) Peng, C. K.; Hausdorff, J. M.; Goldberger, A. L. Fractal Mechanisms in Neural Control: Human Heartbeat and Gait Dynamics in Health and Disease. In *Self-Organized Biological Dynamics and Nonlinear Control*; Walleczek, J., Ed.; Cambridge University Press: 2000; pp 66−96.
(42) Rutherford, K. M.; Haskell, M. J.; Glasbey, C.; Lawrence, A. B. The Responses of Growing Pigs to a Chronic-Intermittent Stress Treatment. *Physiol. Behav.* **2006**, *89*, 670−680.
(43) Kantelhard, J. W.; Koscielny-Bunde, E.; Rego, H. H. A.; Havlin, S.; Bunde, A. Detecting Long-Range Correlations with Detrended Fluctuation Analysis. *Physica A* **2001**, *295*, 441−454.
(44) Milotti, E. 1/F Noise: A Pedagogical Review. arXiv:physics/0204033, 2002.
(45) Hoop, B.; Peng, C. K. Fluctuations and Fractal Noise in Biological Membranes. *J. Membr. Biol.* **2000**, *177*, 177−185.
(46) Laemmli, U. K. Cleavage of Structural Proteins During the Assembly of the Head of Bacteriophage T4. *Nature* **1970**, *223*, 680−685.
(47) Perillo, M. A.; Garcia, D. A.; Marin, R. H.; Zygadlo, J. A. Tagetone Modulates the Coupling of Flunitrazepam and Gaba Binding Sites at Gabaa Receptor from Chick Brain Membranes. *Mol. Membr. Biol.* **1999**, *16*, 189−194.
(48) Yammamura, H. I.; Enna, S. J.; Michael, J. K. *Neurotransmiter Receptor Binding*; Raven: New York, 1978.
(49) Lowry, O. H.; Rosebrough, N. J.; Farr, A. L.; Randall, R. J. Protein Measurement with the Folin Phenol Reagent. *J. Biol. Chem.* **1951**, *193*, 265−275.
(50) Sokal, R.; Rohlf, F. *Introduction to Biostatistics*; W. H. Freeman & Company: New York, 1987.
(51) Durr, A. C.; Schreiber, F.; Ritley, K. A.; Kruppa, V.; Krug, J.; Dosch, H.; Struth, B. Rapid Roughening in Thin Film Growth of an Organic Semiconductor (Diindenoperylene). *Phys. Rev. Lett.* **2003**, *90*, 016104.
(52) De Robertis, E. The Synaptosome. Two Decades of Cell Fractionation of the Brain. In *Neural Transmission, Learning and Memory*; Raven Press: New York, 1983.
(53) Savageau, M. A. MichaelisMenten Mechanism Reconsidered] Implications of Fractal Kinetics. *J. Theor. Biol.* **1995**, *176*, 115−124.
(54) Miller, P. S.; Aricescu, A. R. Crystal Structure of a Human Gabaa Receptor. *Nature* **2014**, *512*, 270−275.
(55) Nusser, Z.; Hájos, N.; Somogyi, P.; Mody, I. Gabaa Receptors Underlies Potentiation at Hippocampal Inhibitory Synapses. *Nature* **1998**, *395*, 172−177.
(56) Kash, T. L.; Trudell, J. R.; Harrison, N. L. Structural Elements Involved in Activation of the Gamma-Aminobutyric Acid Type a (Gabaa) Receptor. *Biochem. Soc. Trans.* **2004**, *32*, 540−546.
(57) Absalom, N. L.; Lewis, T. M.; Schofield, P. R. Mechanisms of Channel Gating of the Ligand-Gated Ion Channel Superfamily Inferred from Protein Structure. *Exp. Physiol.* **2004**, *89*, 145−153.
(58) Chakrapani, S.; Bailey, T. D.; Auerbach, A. Gating Dynamics of the Acetylcholine Receptor Extracellular Domain. *J. Gen. Physiol.* **2004**, *123*, 341−356.
(59) Chakrapani, S.; Auerbach, A. A Speed Limit for Conformational Change of an Allosteric Membrane Protein. *Proc. Natl. Acad. Sci. U.S.A.* **2005**, *102*, 87−92.
(60) Keramidas, A.; Kash, T. L.; Harrison, N. L. The Pre-M1 Segment of the Alpha1 Subunit Is a Transduction Element in the Activation of the Gabaa Receptor. *J. Physiol* **2006**, *575*, 11−22.
(61) Tierney, M. L. Insights into the Biophysical Properties of Gaba(a) Ion Channels: Modulation of Ion Permeation by Drugs and Protein Interactions. *Biochim. Biophys. Acta* **1808**, 667−673.
(62) Yoshimura, K.; Sokabe, M. Mechanosensitivity of Ion Channels Based on Protein-Lipid Interactions. *J. R Soc., Interface* **2010**, *7*, S307−S320.
(63) Casado, M.; Ascher, P. Opposite Modulation of Nmda Receptors by Lysophospholipids and Arachidonic Acid: Common Features with Mechanosensitivity. *J. Physiol* **1998**, *513*, 317−330.

DOI: 10.1021/la5042986
Langmuir XXXX, XXX, XXX−XXX